THE ASTROPHYSICAL JOURNAL, 248:18–37, 1981 August 15

NEAR-MILLIMETER SPECTRUM OF THE MICROWAVE BACKGROUND

DAVID P. WOODY AND PAUL L. RICHARDS
Department of Physics, University of California; and Materials and Molecular Research Division, Lawrence Berkeley Laboratory
Received 1980 August 27; accepted 1981 March 2

ABSTRACT

A complete description is given of a measurement of the spectrum of the cosmic microwave background (CMB). A fully calibrated, liquid helium cooled, ballon borne spectrophotometer was used to measure the emission spectrum of the night sky over the frequency range from 1.7 to 40 cm^{-1}. Great care was taken with the instrumental design to avoid radiation from the Earth or the apparatus. The apparatus was calibrated using a blackbody source with a variety of temperatures before and after the flight. The atmospheric emission was subtracted by fitting the data to the spectrum computed from an atmospheric model. The resulting spectral measurements have a flux accuracy of better than 10% of the peak flux of a 3 K blackbody and extend over the frequency range from 2.5 to 24 cm^{-1}. They show that the spectrum of the CMB peaks at 6 cm^{-1} and is approximately that of a blackbody out to several times that frequency. Some deviations from blackbody shape are observed. The measured flux is equivalent to that from a blackbody in the temperature range from 2.88 to 3.09 K. These measurements are combined with previous observations of the CMB to produce a set of data covering three decades in frequency. This data set is compared with various models of the CMB.

Subject heading: cosmic background radiation

I. INTRODUCTION

The spectrum of the cosmic microwave background radiation (CMB) has been a subject of active experimental investigation ever since its discovery (Penzias and Wilson 1965). Because of the relative transparency of the atmosphere and the availability of microwave receivers, the low frequency (Rayleigh-Jeans) region of the spectrum was explored first. Direct measurements of the spectrum of the CMB in the near-millimeter region at and beyond the peak at ~6 cm^{-1} have proved more troublesome for several important reasons. The background radiation must be measured in the presence of emission from nearby sources including the atmosphere, the Earth, and the apparatus. The ratio of the brightness of a 300 K blackbody to that of a 3 K blackbody is 10^2 at low frequencies. Because of the exponential cutoff of the 3 K curve, however, this ratio is 6×10^2 at 6 cm^{-1} and 1.5×10^5 at 20 cm^{-1}. Avoidance of the emission from ambient temperature objects thus becomes extremely difficult. In practice, high frequency experiments must use liquid helium (LHe) temperature apparatus.

The density and strength of emission lines in the Earth's atmosphere increase rapidly with frequency. Consequently, ground-based measurements can be made at 1 cm^{-1} with a relatively small atmospheric correction. By 12 cm^{-1}, however, large atmospheric corrections are required for measurements made from the highest available balloon altitudes.

The technology for high frequency CMB measurements was and is relatively undeveloped. Because heterodyne receivers with adequate performance were not available, infrared techniques have been used. Early high frequency experiments simply did not have the technology base required. Despite intensive and imaginative efforts, misleading results were sometimes announced. In retrospect, the value of many of these early experiments lay in their contributions to measurement technology. This development has been discussed by Richards (1980) and by Richards and Woody (1980).

Some of the most successful early experiments to measure the CMB at and beyond the peak were done from a balloon (Muehlner and Weiss 1973*a*, *b*). By using an infrared photometer with several relatively wide passbands they were able to demonstrate that the spectrum of the CMB did not continue to rise beyond 6 cm^{-1}. Uncertainties in the correction for the emission of the residual atmosphere at balloon altitude, however, prevented observation of the decrease of the spectrum at higher frequencies.

In this paper we report the results of a series of experiments which make use of a fully calibrated balloon-based spectrophotometer to measure the spectrum of the CMB at and beyond the peak. The first measurements in this series were reported by Woody *et al.*

(1975) and by Woody (1975). A preliminary report of a second experiment using improved apparatus was given by Woody and Richards (1979). In this paper we give a full account of this second measurement. The design and testing of the apparatus are described in §§ II and III, the flight procedures in § IV, and the analysis of the data in §§ V and VI. An attempt has been made to make the paper sufficiently complete that the reader can understand the nature of all the important experimental problems and the approach that was used in solving them. Although this detailed description is unusual in astrophysical literature, we believe that only in this way can the reader properly evaluate the significance of the experimental results.

The observations of the CMB now cover the frequency range from 0.014 to 14 cm^{-1}. The measurements have sufficient accuracy to warrant testing them for deviation from a simple Planck spectrum. The consistency of the observations is examined in § VII. The data fit a simple Planck spectrum remarkably well, but deviations are apparent. Attempts to obtain a better fit using various models for deviations from a blackbody spectrum are described in § VIII.

II. INSTRUMENT DESCRIPTION

A diagram of the balloon-borne spectrophotometer developed to measure the CMB is shown in Figure 1. The instrument was designed to minimize stray radiation from the Earth and nearby warm objects, and to eliminate emission from the apparatus itself. Other design goals included sufficient resolution to allow subtraction of the atmospheric emission from the observed spectrum and enough sensitivity to measure the CMB to an accuracy of a few percent in a few hours. The principal features of the instrument are a ^{3}He cooled detector A, a Fourier transform spectrometer B, and a conical antenna C with an apodizing horn D and a large ground plane E. The whole instrument, including the beam defining part of the antenna C, is cooled by immersion in LHe. The chopper F between the spectrometer and the detector compares the collected radiation against that emitted by a blackbody at the temperature of the LHe bath.

The detector A was a composite bolometer developed specifically for this measurement (Nishioka, Richards, and Woody 1978). The low radiation power levels ($<10^{-11}$ W) allowed us to exploit the improved sensitivity which can be achieved by cooling bolometers to ~0.3 K. The bolometer used had an electrical noise equivalent power of 6×10^{-16} W $Hz^{-1/2}$ and a time constant of 6 ms. The collecting area was 0.25 cm^2 with a 50% absorption efficiency. The 0.36 K heat sink temperature for the bolometer was provided by a single-shot ^{3}He evaporation refrigerator G utilizing a Xelite™ absorption pump H.

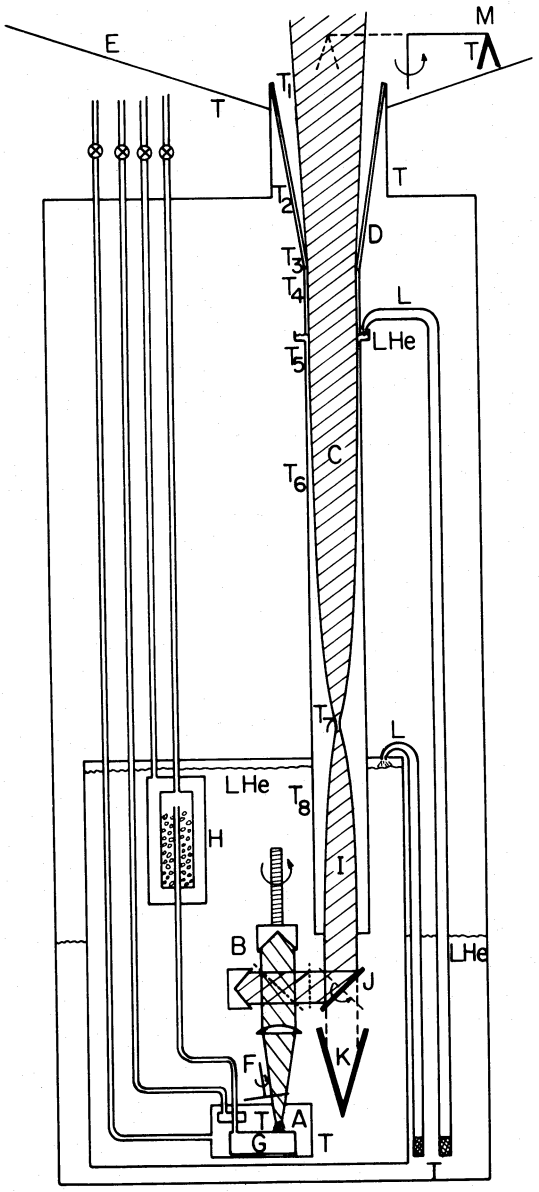

FIG. 1.—Diagram of the spectrophotometer. Optical components are shown to scale and other components are shown schematically: A, ^{3}He cooled detector; B, Fourier transform spectrometer; C, LHe cooled antenna; D, apodizing horn; E, ground plane; F, chopper; G, ^{3}He boiler; H, ^{3}He absorption pump; I, collimator; J, diagonal mirror; K, blackbody; L, superfluid LHe fountain-effect pump; M, in-flight calibrator; T, thermometers.

The spectrometer B was a Polarizing Michelson Interferometer (PMI) (Martin and Puplett 1969). The theory and operation of PMIs are described by Lambert and Richards (1978). The construction and performance of the flight instrument have been described by Woody (1975). A free standing wire grid polarizer was used as a broad-band, high-efficiency beamsplitter. The measured

on-axis efficiency of the PMI was more than 95% over the range from 2 to 30 cm^{-1}.

The PMI was operated in the "step and integrate" mode, with a rotating polarizing chopper with eight polarizing segments and synchronous demodulation of the signal. In this instrument the observed inteferogram (signal versus interferometer path difference) oscillates around the electrical zero. This has the advantage that source intensity or detector responsivity changes did not appear as spectral features to first order. The maximum travel of the movable mirror was 3.72 cm from zero path difference, which gave a nominal resolution of 0.13 cm^{-1}. Both the chopper and the screw drive for the interferometer mirror were connected by shafts to ambient temperature motors at the top of the apparatus.

The radiation collected by the antenna was collimated by an inverted conical flux concentrator I (Winston 1970) and reflected off a diagonal mirror J into the PMI. The diagonal mirror could be tilted so that the PMI received radiation from a blackbody K immersed in the helium bath. This was used to test for electrical offsets and stray light leaks.

The antenna was probably the single most important part of the instrument. It had to collect radiation from a well defined beam on the sky and keep the stray radiation from the Earth and the lower atmosphere well below the level of the CMB. The radiation emitted into the spectrometer by the antenna also had to be much smaller than the CMB signal. These requirements are quite severe because a 3 K blackbody approaches the Wien limit at frequencies above 6 cm^{-1} so that the brightness decreases exponentially with frequency, while ambient temperatures objects are still in the Rayleigh Jeans limit.

Our antenna consisted of three components: a Winston flux concentrator C, an apodizing horn D, and a large ground plane or earthshine shield E. The Winston concentrator determined the system throughput of 0.25 sr cm^2 and the beam pattern on the sky in the limit of geometric optics. It was electroformed from copper with a 6.0 cm entrance diameter, a length of 58.2 cm, and small exit hole 0.32 cm in diameter. The geometric beam profile had a sharp cutoff at 3°.1 off-axis. The Winston concentrator was cooled by the use of superfluid LHe fountain-effect pumps L. The temperature of the top was kept below 7 K. The apodizing horn D decreased the sidelobes by reflecting the diffracted rays back into the forward beam direction. The horn was outside the geometrical beam and extended from the top of the cooled Winston concentrator to the top of the cryostat. The horn surface was a laminate of stainless steel, copper, and polyethylene (Woody 1975). This material had extremely low emissivity and low thermal conductance. The top of the horn was covered with a Mylar window to keep frost out during ground operations. Once float attitude was reached, the window was removed and He boil-off gas was allowed to escape through the antenna. The ground shield E was an aluminum collar with radius greater than 1 m around the top of the apparatus. This prevented the diffraction back-lobes from seeing the Earth and the lower atmosphere.

An extensive program of calculations and measurements was undertaken to characterize the antenna. Many of the measurements were done with an earlier version of the antenna which used a straight cone in place of the Winston concentrator. The antenna pattern for a Rayleigh-Jeans source with our bandpass was measured using a novel technique (Mather, Richards, and Woody 1974). The result is shown in Figure 2 for the straight cone and apodizing horn combination. These measurements are compared with calculations based upon a scalar version of the geometrical theory of diffraction (Keller 1962). The calculations started with a uniform random distribution of several million rays at the small end of the antenna and traced the rays as they propagated out of the antenna toward the sky. Diffraction corrections were applied when a ray crossed the transition between the cone and the horn, and again when it passed through the entrance plane of the horn. At angles beyond 1 radian an analytic continuation of the ray tracing results was used which was based upon the exact solution for diffraction from a circular aperture. The agreement between the measurements and calculations gives us confidence that we can apply the calculations to similar antenna structures. The calculations for the Winston concentrator and apodizing horn combination used in this experiment are also shown in Figure 2.

The calculated response from the Earth at 12 cm^{-1} with the antenna pointed at a zenith angle of 25° is 50 times smaller than that from the peak of a 3 K blackbody filling the main beam. This was marginally sufficient for our purposes, and the ground plane was added to reduce the response at large angles. It was estimated from knife-edge diffraction theory to reduce the earthshine by another factor of 20. With the ground plane in place, radiation from below the horizon must be diffracted three times before reaching the spectrophotometer. Consequently, the spectrum of the diffracted earthshine is expected to be changed from ν^2 to approximately ν^{-1}.

The antenna emission was determined from laboratory measurements and calculations which were substantiated by in-flight tests. The expected emission for various temperature profiles was calculated by including an angle-dependent emissivity in the ray tracing program. An independent measurement was made of the emissivities of the Winston cone and apodizing horn. This was done by plugging the openings of the cone-horn combination and measuring the Q of the resulting integrating cavity with a laboratory Fourier spectrometer. The angular average of the emissivity computed from these measurements agreed with the emissivity calcu-

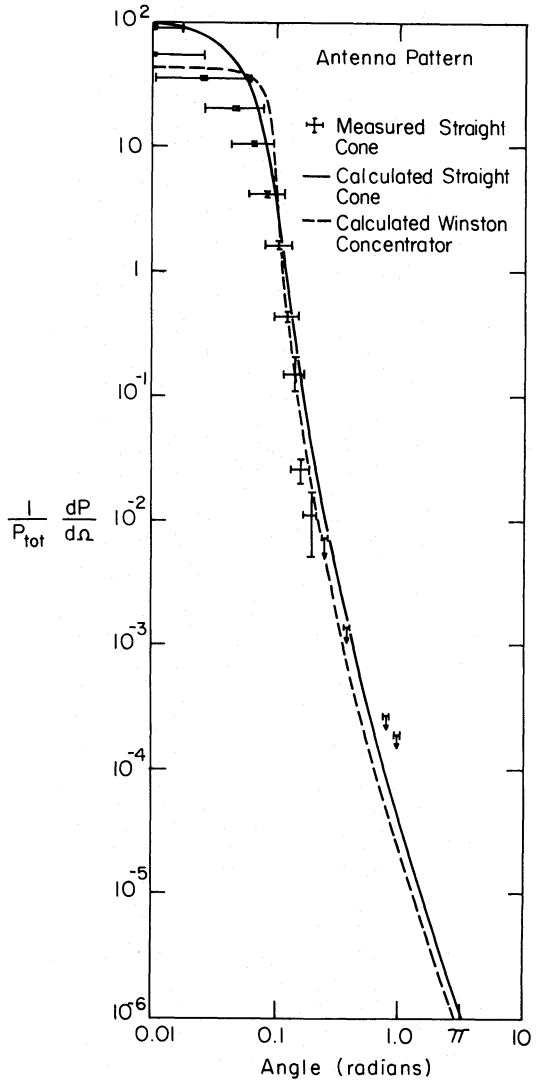

FIG. 2.—Comparison of antenna patterns measured and calculated for a straight-cone antenna and calculated for a Winston concentrator antenna.

lated from the measured dc conductivity of the copper. The calculations were checked during an earlier flight by increasing the temperature of the top of the beam-defining cone from 4 K to 26 K. A small increase in signal was observed which agreed with the calculations. The expected radiation from the cooled antenna system based upon these tests increases monotonically from 4×10^{-14} W/cm^2 sr cm^{-1} at 2.5 cm^{-1} to 14×10^{-14} W/cm^2 sr cm^{-1} at 15 cm^{-1}. It arose nearly equally from the cone and the horn. This estimated contribution is small enough that no correction to the measurement is required.

The telemetry requirements were met by an 8,000 bit per second pulse-code modulated data system and a 40 command tone-reed command system. The commands included zenith angle control, interferometer scan length, internal mirror position, and amplifier gain. The bolometer output was amplified, digitized, and telemetered to the ground. The 17 Hz reference signal derived directly from the chopper shaft was similarly treated. There were 48 channels of housekeeping information including the monitoring of the bolometer voltage, heat sink temperature, and temperatures at 17 other places on the apparatus, indicated by the symbol T in Figure 1.

The telemetry bit stream was recorded on digital tape at the ground station and simultaneously converted to analog signals for real-time monitoring of the experiment. A lock-in amplifier which was interfaced to a minicomputer was used to synchronously demodulate the signal. The computer Fourier transformed individual interferograms to give spectra during the balloon flight. This real-time monitoring together with the 40 commands gave us excellent interactive control of the experiment.

III. CALIBRATION

An important part of any measurement of the CMB is the calibration of the instrument. The operation of the spectrophotometer was monitored before, during, and after the flight to verify that its performance remained unchanged. The most extensive calibrations were carried out after the flight using a variable low temperature blackbody source inserted into the Winston cone C. The primary calibration of the scale factor was obtained from spectra measured with a blackbody temperature of 20.14 K which was high enough to give a good signal over the whole frequency range of interest, but low enough to avoid saturation effects in the detector. An ambient ^{4}He temperature absorbing plug inserted into the antenna was used to verify that zero electrical signal corresponded to zero optical signal.

Consistency tests were carried out before and after the flight by using the room as a ~300 K blackbody source. Such a bright source saturated the detector so that its response was nonlinear. It was still possible to compare the responsivity before and after the flight. The ratio of these responsivities is shown in Figure 3. The average value of the ratio of these quantities was 1.01. The ratio in the range from 3 to 30 cm^{-1} contained slow oscillations with rms value less than 3%, presumably due to small differences in interferometer alignment.

A small ambient temperature blackbody source M was used to check the responsivity during the flight. Its small size and varying (but known) temperature made it a poor absolute calibrator. It was used to check the performance of the instrument with ±20% accuracy. A more accurate and reliable check on performance was obtained by monitoring the bolometer operating param-

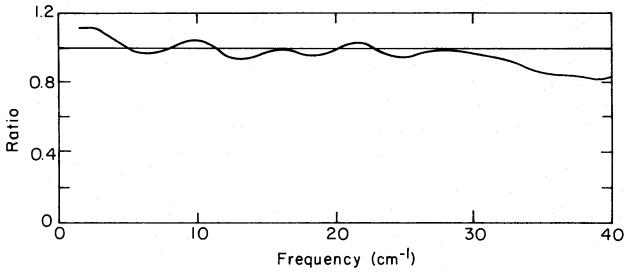

FIG. 3.—Postflight spectrophotometer calibration divided by preflight calibration.

eters: the ^{3}He heat sink temperature, the bias current, and the dc bias voltage. These parameters remained steady during the flight and had the same values as were measured in laboratory tests done at the same ^{4}He bath temperature and radiation loading.

Figure 4 is a scale drawing of the blackbody source used for the primary calibration after the flight. It consists of a grooved Eccosorb MF-110^{TM} absorber attached to a copper heat sink and mounted inside a vacuum can. The absorber and heat sink assembly could be regulated at temperatures ranging from 4 to 20 K using a calibrated germanium thermometer and a heater. A separate thermometer was used to monitor the temperature of the front surface of the absorber. Low temperature thermal conductance and infrared transmittance data were used to estimate the performance of this system. The absorber temperature was known to $\pm 1\%$, and its emissivity was found to vary from more than 99% at 20 cm^{-1} to 98% at 2 cm^{-1}. The window emission and diffraction effects were negligible. When the multipass characteristic of the cavity formed by the Winston concentrator and calibrator are included, the emissivity-temperature product of the calibrator was within $(+2.7, -2.5\%)$ of the temperature determined by the germanium thermometer throughout the frequency range of interest.

The calibration procedure was checked by measuring spectra with the blackbody source at several temperatures such that the spectral range of the instrument included both Rayleigh-Jeans and Wien portions of the Planck curve. Figure 5 shows a set of low resolution spectra measured with the calibrator at temperatures of 5.44, 10.34, and 20.14 K while the ^{4}He bath reference temperature was 1.7 K. The instrumental responsivities determined from these measurements all agreed to within a few percent even for spectra measured many days apart.

Appendix A describes a method for using these spectra to independently compute values for both the calibrator emissivity and temperature and/or the stray light leakage, without reference to the thermometer calibration. The emissivity and temperature determined this way were consistent with the direct measurements.

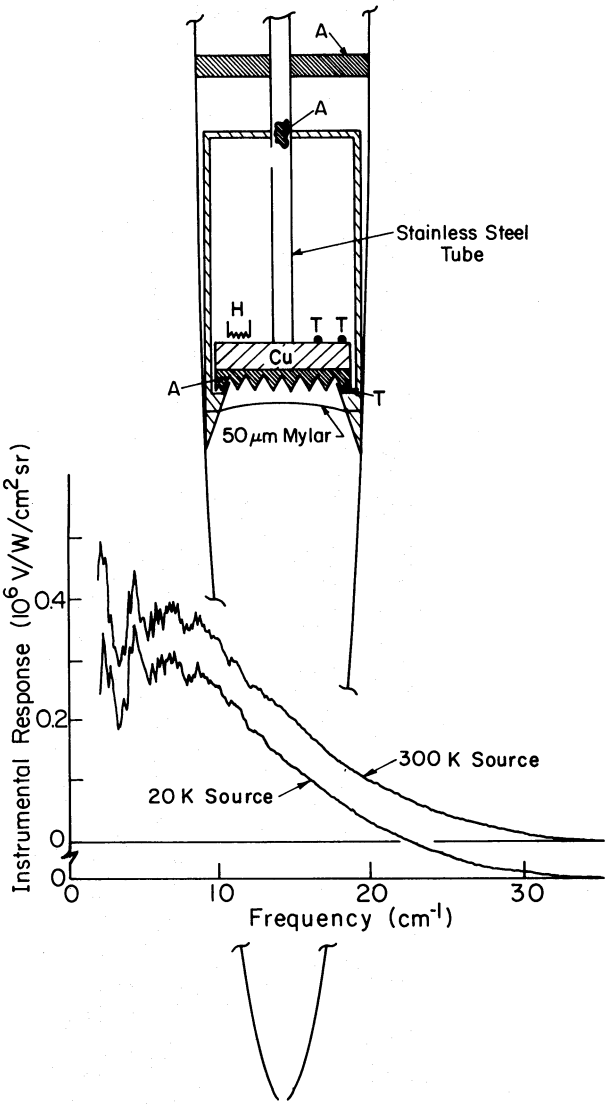

FIG. 4.—Cold blackbody source used for laboratory calibrations inserted in the upper portion of the cooled antenna: T, thermometers; A, absorbers; H, heater. The absolute instrumental calibration obtained by operating this source at 20 K is compared to a calibration obtained by using the laboratory room as a 300 K source.

The uncertainty was $\pm 5\%$ which arose from noise in the spectra measured for the lowest calibrator temperature. The limit on stray radiation leakage was less than 2% of the peak of a 3 K blackbody.

The instrumental responsivity is shown in Figure 4. This measurement is based on three high-resolution measurements of the cold calibrator at 20.14 K. The higher temperature spectra were used because of their better signal-to-noise ratio, particularly at the high frequency end of the spectrum. The sharp features ap-

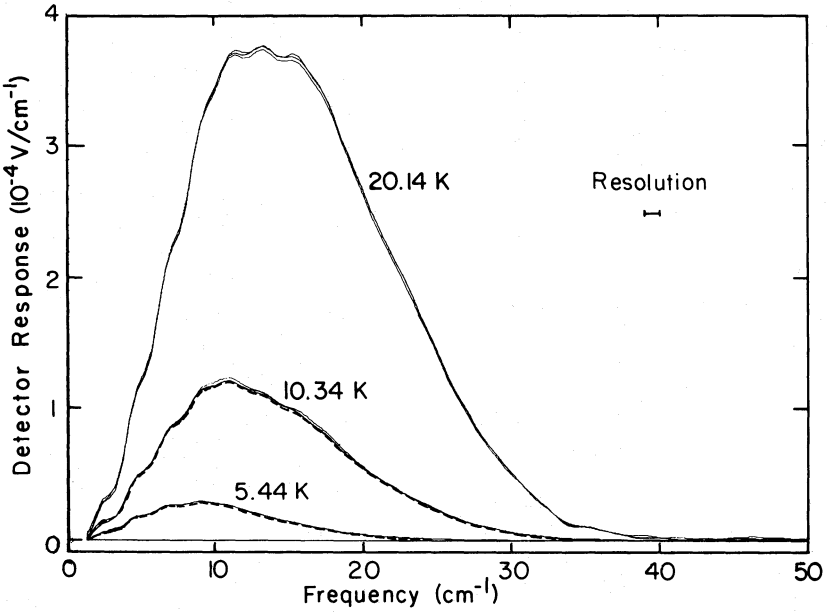

FIG. 5.—Measured spectra of the cold blackbody calibrator: Three spectra with the calibrator at 20.14 K, three at 10.34 K, and two at 5.44 K. The dashed curves are the calculated detector response for 5.44 K and 10.34 K blackbodies when the 20.14 K spectra are used to calibrate the instrument.

parent at low frequencies are reproduced in all of the spectra and are a result of the mode structure of the antenna-spectrometer combination. The low frequency response is limited at 1.5 cm^{-1} by the waveguide cutoff from the 0.32 cm diameter exit aperture in the Winston concentrator. The high frequency response is rolled off by a Fluorogold™ filter.

The spectra measured with the calibrator at 5.44 and 10.34 K were used to determine the internal consistency of the calibration procedure. The dashed curves in Figure 5 show the expected response to 5.44 and 10.34 K blackbodies when the instrumental responsivity determined from the 20.14 K spectra is used. The best fit blackbody temperature is 5.52 K for the 5.44 K calibrator spectra and 10.39 K for the 10.34 K calibrator spectra. The internal consistency is thus well within the $(+2.7, -2.5\%)$ uncertainty in the emissivity temperature product.

An additional check on the spectral shape of the instrumental response was provided by measuring the spectrum of the room as a ~300 K blackbody. Although under normal bias conditions a 300 K source saturated the detector and gave a nonlinear response, the response could be linearized with some sacrifice in responsivity by increasing the bias current by one order of magnitude. The instrumental responsivity, corrected for the change in bias current, that was obtained from the 300 K source is shown in Figure 4 along with that obtained using the cold calibrator. This test confirmed that the structure of the electromagnetic modes which entered the instrument from the room (or the sky) was very similar to that measured with the cold calibrator in place. It also provided a useful test for variation of the emissivity of the cold calibrator with frequency. Uncertainties in the responsivity correction for the change in bias current makes the 300 K source a poor absolute calibrator.

The errors in the instrumental responsivity can be divided into two types: those which are independent of frequency, and those which are uncorrelated across the spectrum. Errors included in the first category are bolometer responsivity (±3%), calibrator temperature and emissivity $(+2.7\%, -2.5\%)$, amplifier gain (±1%), telemetry level encoding and decoding (±1%), and the effect of the varying liquid helium level inside the Winston concentrator $(+0, -5.4\%)$. The rms sum of these errors is $+4, -7\%$ with the asymmetry resulting from our knowing the liquid level inside the Winston concentrator during the laboratory calibration but not during the flight. Errors we have included in the second category include noise on the calibration spectrum $(\pm 7/\nu\%)$ (where ν is the frequency in cm^{-1}) and small spectral shape differences observed before and after the flight (±3%). The sum of these errors is $(3+7/\nu)$ %.

IV. FLIGHT DESCRIPTION

The spectrophotometer was mounted in a balloon gondola along with the associated telemetry and battery pack. A schematic diagram of the flight configuration is shown in Figure 6. The zenith angle of the spectrophotometer was controlled by a motor and ball screw and

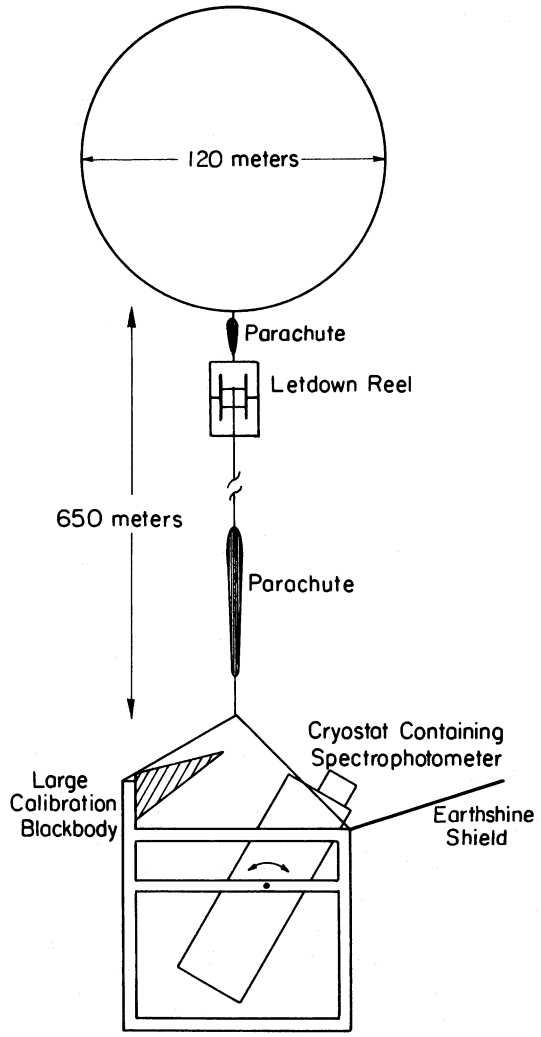

FIG. 6

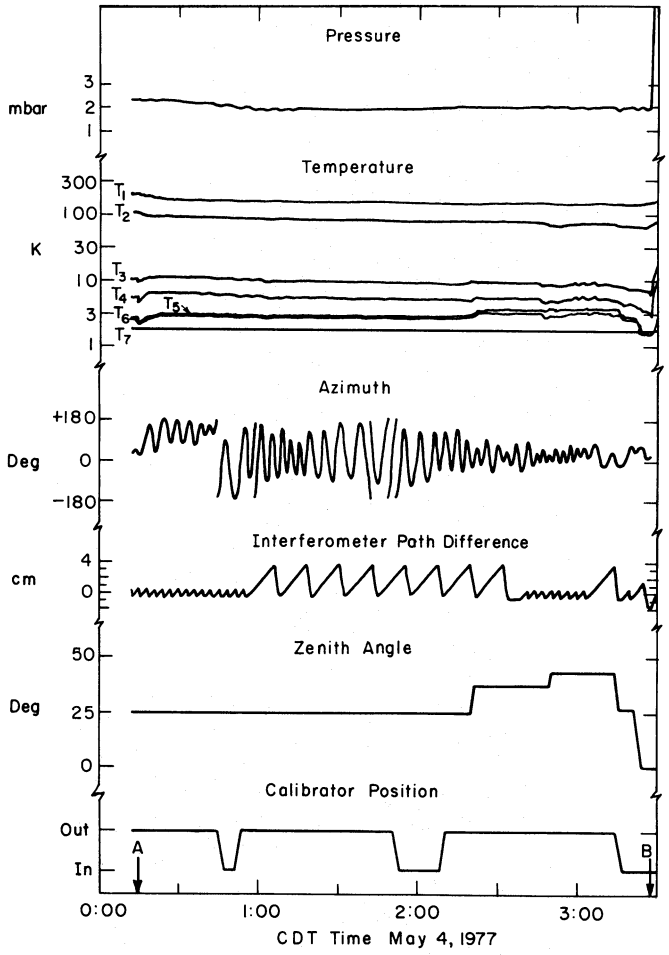

FIG. 7

FIG. 6.—Configuration of the flight-train

FIG. 7.—Selected housekeeping data. The window was opened at time A, and the flight was terminated at time B. Thermometers T_1 through T_7 are located at various positions on the antenna as indicated in Fig. 1. The thermometer T_8, which was immersed in the LHe bath, gave the same reading as T_7.

was varied from vertical to 45°. The azimuthal orientation was not controlled, but was monitored by two magnetometers on the gondola. The gondola was lowered 650 m below the balloon after the launch by a let-down reel (Muehlner and Weiss 1973*a*). This was done to keep the 8.5×10^5 m^3 balloon well out of the field of view.

The system was launched from Palestine, Texas, at 19:40 CDT on 1977 May 3. A float altitude of 43 km was reached at 0:15 on May 4, at which time the protective window over the antenna was removed and measurements of the night sky emission were started. The flight was terminated at 3:28 when the balloon reached the Gulf of Mexico near Baytown, Texas.

The instrument performed very well during the flight. The time dependence of a portion of the housekeeping data, including the temperatures of several points on the antenna, the ambient pressure and the orientation, are presented in Figure 7. The region of the sky swept out by the 6° beam is shown in Figure 8. The signal-to-noise ratio on a spectrum computed in real time from a single 3 minute interferogram was sufficient to easily identify the CMB and the major atmospheric features.

A total of 25 interferogram scans were measured at various zenith angles and resolutions. Five more scans were recorded to characterize the instrument by observing with the small calibration body M in the field-of-view and with the diagonal mirror J flopped to observe the

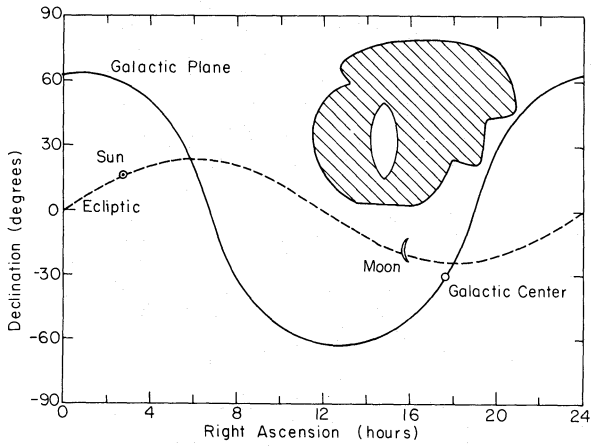

FIG. 8.—Equatorial map showing the portion of the sky covered by the observations.

reference blackbody in the liquid helium bath. The scans of the sky were divided into 15 at a zenith angle of 25°, five at 36°, and five at 43°. The optimum observing angle of 25° was set as a compromise between the effects of atmospheric emission at large angles and the contribution from the balloon and the flight train at small angles. Measurements at larger angles were made to test the model of the atmosphere used to fit the data and to check for earthshine contamination. Interferogram points were measured at path difference intervals of 8.2×10^{-3} cm and integrated for 0.936 s. In 16 short 128-point scans the path difference was varied from −0.484 cm to +0.574 cm. In nine long 512 point scans the range covered was from −0.484 to +3.721 cm. Thus, 22% of the time was spent in scans giving a nominal resolution (equal to the inverse of twice the maximum path difference) of 1.03 cm^{-1}, 17% with a nominal resolution of 0.87 cm^{-1} and 61% with a nominal resolution of 0.13 cm^{-1}. This division of integration time was a compromise between obtaining good signal-to-noise on the broad CMB and sufficient resolution to identify and separate the atmospheric emission lines and to check for unexpected line features.

V. DATA REDUCTION

The digital recording of the raw telemetry bit stream was used for all of the postflight data processing. Programs were written to decode and plot the housekeeping data as a function of time. Programs were also written to process the detector, chopper reference, and interferometer position signals. They included a digital lock-in program which synchronously demodulated the detector signal in phase with the chopper and integrated the resultant demodulated signal for 0.936 s at each interferogram point. The output from this lock-in program was an interferogram for each scan of the interferometer mirror. Data points measured while the zenith angle and calibrator motors were running were eliminated, as were points interrupted by telemetry dropouts. All other data points were included.

The individual interferograms were phase corrected for linear and quadratic phase errors. The linear error corresponded to a missampling of the interferogram (i.e., not having a sample point exactly at zero path) by 14 μm, or 0.18 of a step length. The quadratic error corresponded to an angular misalignment of the interferometer (Goorvitch 1975) of 2.6×10^{-3} rad. The magnitudes of the corrections were determined by a fitting program which minimized the rms value of the sine transform of the interferogram. The rms value of the sine transform after phase correction was only 3 times larger than the noise and contained less than 1% of the power in the cosine transform. This procedure was thought to be preferable to the usual blind calculation of the phase correction (Bell 1972, chap. 12) because it gave a useful check on the operation of the interferometer.

A statistical analysis of the noise was carried out by comparing the signal at the same sampling point for successive scans after correcting for slow float altitude variations. The points had a nearly Gaussian distribution which was 8 times larger than the expected detector noise. This factor is in good agreement with a calculation of the digitizing noise in our 8-bit telemetry system. The signal-to-noise on the zero path point, which is proportional to the intergrated spectral power, was 50 for a single scan.

The scans were divided into groups according to the observing conditions. The scans at 36° and 43° each formed one group, while the scans at 25° were divided into groups according to ambient float pressure. This gave five final interferograms measured at different air masses with sufficient signal-to-noise to test for correlations. Since the PMI with polarization chopping gives a signal which is modulated about zero, a slow variation in total signal has only a second order effect on the spectral shape. Thus the changing atmospheric contribution due to float altitude variations had a negligible effect on the CMB part of the spectrum. The primary interferogram used for determining the CMB was obtained by averaging all of the 25° scans together. The 15 individual interferograms are shown superposed in Figure 9.

Spectra were obtained by Fourier transforming the interferograms after multiplying by an apodization function of the form

$$A(x)=\left[1-(x/x_{\max})^2\right]^2. \quad (1)$$

The normalized resolution function for this apodization is

$$a(\nu, x_{\max})=\frac{16x_{\max}}{\alpha^3}\left[\left(\frac{3}{\alpha^2}-1\right)\sin\alpha-\frac{3}{\alpha}\cos\alpha\right], \quad (2)$$

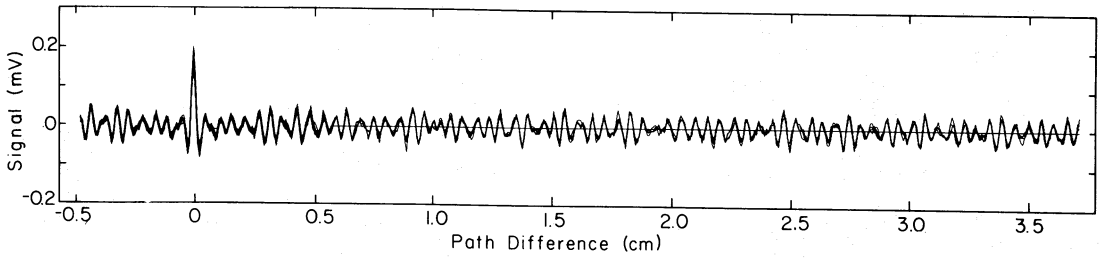

FIG. 9.—Superposition of 10 short interferograms and 5 long interferograms measured at the zenith angle of 25°

where $\alpha \equiv 2\pi\nu x_{\max}$. The apodization function is asymmetric when the maximum negative path difference, $x_{\max-1}$, is unequal to the maximum positive path difference, $x_{\max-2}$. The resolution function then becomes

$$a(\nu, x_{\max-1}, x_{\max-2}) = \tfrac{1}{2}[a(\nu, x_{\max-1}) + a(\nu, x_{\max-2})]. \quad (3)$$

VI. DATA ANALYSIS

This section describes the recovery of the flux of the CMB from the observed night sky emission spectrum shown in Figure 10*a*. The general blackbody character of the CMB is seen in this raw spectrum without any further analysis. It is a broad continuum which peaks at 6 cm^{-1} and decreases at higher frequencies. In order to see the CMB above $\nu \approx 10$ cm^{-1}, it was necessary to subtract the atmospheric contribution.

The atmospheric contribution was determined by fitting a model of the atmospheric emission from molecular H_2O, O_3, and O_2 to the observed spectrum. The emission from known minor constituents is expected to be negligible at the altitude of our observations. The molecular line parameters for H_2O and O_3 were obtained from the AFCRL Atmospheric Line Parameter Compilation (McClatchy *et al.* 1973). The line parameters for the set of O_2 lines at 2 cm^{-1} are accurately known (Liebe, Gimmestad, and Hopponen 1977). The parameters for the higher frequency lines are based on perturbation calculations (Tinkham and Strandberg 1955; Gebbie, Burroughs, and Bird 1969; Kakar 1977)

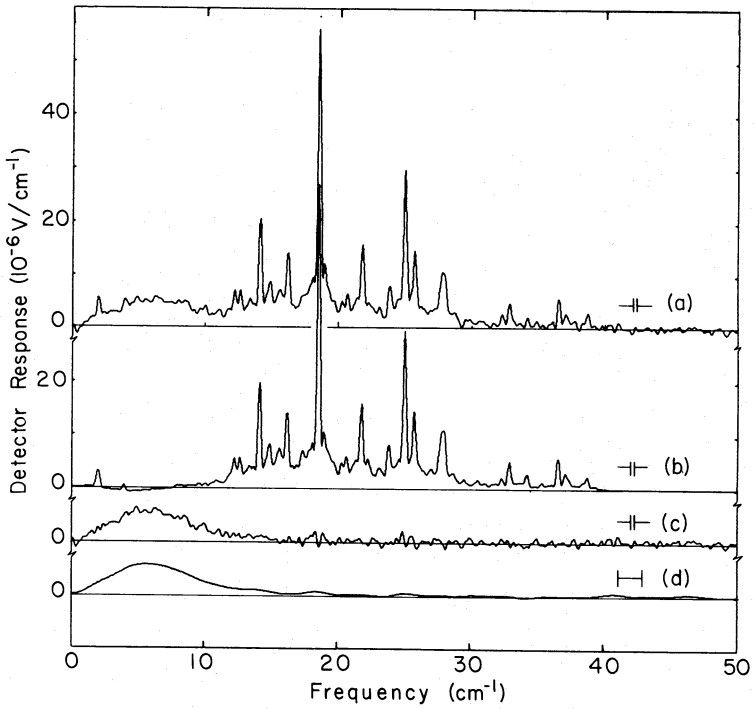

FIG. 10.—(*a*) Observed response of the spectrophotometer to the night sky. (*b*) Calculated response of the spectrophotometer to the atmosphere, including the effect of the 1.67 K reference temperature. (*c*), (*d*) Response to the CMB at two different spectral resolutions obtained by subtracting (*b*) from (*a*).

using the measured microwave parameters. The model assumed that the atmosphere was isothermal, uniformly mixed and had an exponential pressure profile. The pressure and temperature are fixed parameters determined by inflight measurements and the U.S. Standard Atmosphere model (1966), respectively. The only free parameters are the mixing ratios or column densities of the emitting molecules; H_2O, O_3, and O_2.

Under our flight conditions the line widths of H_2O and O_3 are dominated by pressure broadening. The Doppler broadening is typically a factor of five smaller. In addition to pressure broadening the effect of the Zeeman splitting in the Earth's magnetic field (Liebe, Gimmestad, and Hopponen 1977) was included as an effective line broadening for O_2. The line widths at the float pressure of 2 mbar were less than 10^{-3} cm^{-1}, which is much less than typical line separations and much less than our experimental resolution. Thus, the lines were not resolved and were not overlapping. In contrast to airplane or mountain top observations, the contribution from the wings of high frequency lines could also be neglected. The power emitted by each line was treated independently using the equivalent line width approximation (Goody 1964, p. 125) which is valid for unsaturated lines or saturated lines which are widely separated. This equivalent width, when multiplied by the blackbody emission at the temperature of the atmosphere, yielded the emitted power. The equivalent widths were calculated in closed form as a function of strength, column density, and width at float pressure using a pressure broadened Lorentzian line shape (Goody 1964, p. 233). The procedure used to calculate the flux emitted by an emission line is described in Appendix B.

The problem of convolving a high resolution calculated line spectrum with the instrumental resolution function was avoided by doing the fits in interferogram space. A simulated interferogram for the atmospheric emission spectrum was obtained by multiplying the power emitted at the frequency of each molecular line by the measured instrumental response function and then computing the Fourier transform. Continuum sources of radiation could also be added to the calculated spectrum and the resulting interferogram. The measured interferogram points were weighted according to amount of averaging time, so as to take proper account of uncertainties due to noise. The fitting was done by minimizing the weighted rms deviation between the measured interferogram and the simulated interferogram with the column densities of the emitting molecules and various continuum parameters as free variables.

The atmosphere is dominated by high-frequency, high-resolution features, whereas the CMB is a low-frequency, broad continuum. The correlation coefficients between the temperature and the emissivity of a blackbody (included in the fit to mimic the CMB) and the column densities were 0.01 for H_2O, 0.08 for O_3, and 0.05 for O_2. A series of fits were done in which different spectral characteristics were emphasized to show that these cross correlations are small enough that the atmospheric contribution could be determined independently of the detailed assumptions about the CMB. These included fitting only to the high frequency data $\nu > 14$ cm^{-1}, and to the high resolution data, $\Delta\nu < 2$ cm^{-1}, and by adding various blackbody and power-law continuum sources to the model. In essence, the quantity of molecular line emission was determined by the data above 18 cm^{-1} where it was large, and the model was used to extrapolate to lower frequencies where the atmospheric contribution was small, but still interfered with the observation of the CMB. The resulting best fit column densities are presented in Table 1 along with the error limits which include both statistical errors and differences between the results from the various fitting procedures.

TABLE 1

FITTED ATMOSPHERIC MODEL PARAMETERS

Molecule	Column Density at 25° Zenith Angle
H_2O	$(2.76 \pm 0.16) \times 10^{17}$ cm^{-2}
O_3	$(1.72 \pm 0.14) \times 10^{17}$ cm^{-2}
O_2	$(1.09 \pm 0.15) \times 10^{22}$ cm^{-2}

The response of the instrument to the atmospheric emission calculated from this model using the best fit column densities is shown in Figure 10*b*. Note that the calculation includes the effect of the finite reference temperature for the spectrophotometer so that the response is negative in the region where the atmospheric emission is less than the emission from a blackbody at the 1.67 K temperature of the LHe bath.

The CMB is obtained by subtracting the atmospheric contribution, Figure 10*b*, from the observed night sky emission, Figure 10*a*. This difference is shown in Figures 10*c* and 10*d* at resolutions of 0.28 cm^{-1} and 1.79 cm^{-1}, respectively. The quality of the atmospheric model can be judged by noting that the rms residual above 20 cm^{-1}, where the CMB is expected to make a negligible contribution, is comparable to the noise, as determined by the spectrum above 40 cm^{-1} where there is no optical signal, and is small compared with the observed spectral intensity. The spectral flux of the CMB is obtained by dividing the difference in Figure 10*c* or 10*d* by the instrumental responsivity in Figure 4. This spectral flux convolved with a 1 cm^{-1} wide triangular resolution function is plotted in Figure 11.

The O_2 emission lines provide a check on the instrumental responsivity determined from the cold blackbody calibration spectra. The mixing ratio and thus the column density of O_2 are known, so that its emission can be calculated from our model with no free parameters.

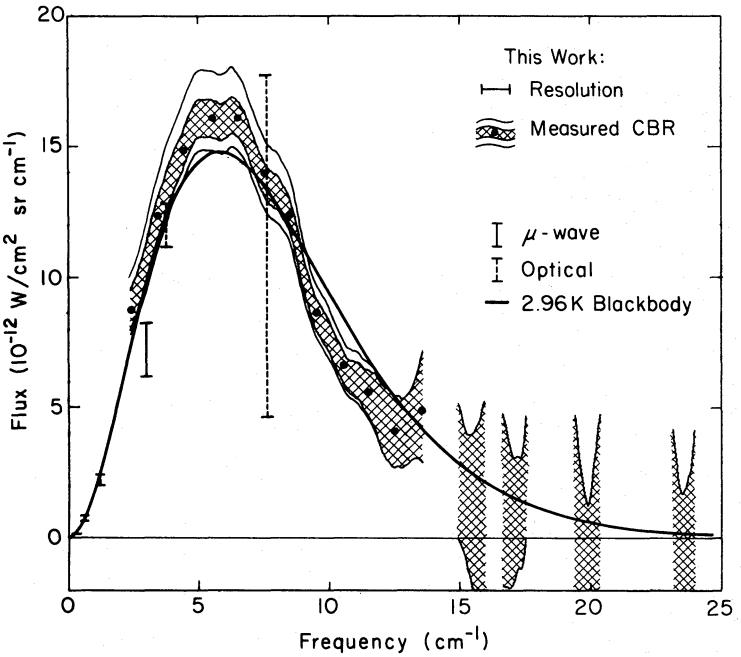

FIG. 11.—Measured spectrum of the cosmic background radiation plotted as ± 1 σ error limits. There are gaps in the data at the frequencies of strong atmospheric emission lines where the errors become very large. The shaded region includes contributions to the error which are uncorrelated across the spectrum. Additional solid lines are shown to represent the effect of changing the frequency-independent scale factor by ± 1 σ. The shaded region can be scaled up or down within these limits. The dots are the measured values given in Table 2. These are separated by the resolution interval of 1.01 cm^{-1} and so are nearly statistically independent. The spectrum of the 2.96 K blackbody, which has the same integrated flux as the measured spectrum, and selected microwave and optical measurements of the CMB are also shown for comparison.

The expected column density based upon a 21% mixing ratio, 25° zenith angle, and 2.18 mbar pressure at float altitude is 1.03×10^{22} O_2 cm^{-2}. This is within the $\pm 14\%$ 1 σ errors on the fitted column density. Since most of the lines are saturated, with the emitted power scaling as the square root of the column density, this gives a check on the accuracy of the overall calibration factor of ± 7 percent.

The calibration can also be checked at the positions of individual O_2 lines by comparing the calculated spectra with the observed O_2 spectrum. Figure 12 *a* shows the measured O_2 spectrum obtained by subtracting the calculated best fit spectra of H_2O, O_3, and a Planck curve with adjustable temperature and emissivity from the sky emission spectrum in Figure 10*a*. The calculated O_2 spectrum for 1.03×10^{22} O_2 cm^{-2} is shown in Figure 12*b*. These spectra are Fourier transforms of unapodized interferograms with nominal resolution of 0.13 cm^{-1}. The ratio of the measured spectrum divided by the calculated spectrum at the postitions of the strong O_2 lines is shown in Figure 11*c*. The error bars are the estimated ± 1 σ errors from the calibration, the molecular line parameters, and the noise in the observed spectrum. The weighted average for the ratio is 1.06 ± 0.06. The accuracy of this technique is limited by the detector noise at the 2 and 4 cm^{-1} groups where the line strengths are accurately known (Liebe, Gimmestad, and Hopponen 1977) but the atmospheric signal is weak and our calibration is relatively poor. At the position of the higher frequency lines, the accuracy is limited by the 10% uncertainty in the calculated line strengths (Gebbie, Burroughs, and Bird 1969; Kakar 1977).

Another source of the inaccuracy in all of our atmospheric fits arises from the structure on the instrumental responsivity shown in Figure 4. This structure arises from individual electromagnetic modes and thus is more pronounced at low frequencies where the number of modes per unit frequency is small. The measurement of the instrumental responsivity probably does not fully resolve this structure, so it does not represent the true response of the instrument for narrow atmospheric lines. This error is reduced somewhat by averaging in cases where the atmospheric line is split into several components.

The error analysis of the CMB flux includes calibration errors, the spectral noise, and errors in the atmospheric model. The calibration errors were discussed in an earlier section and are of two types: those which are essentially uncorrelated from one spectral point to the next, and those which are correlated across the spec-

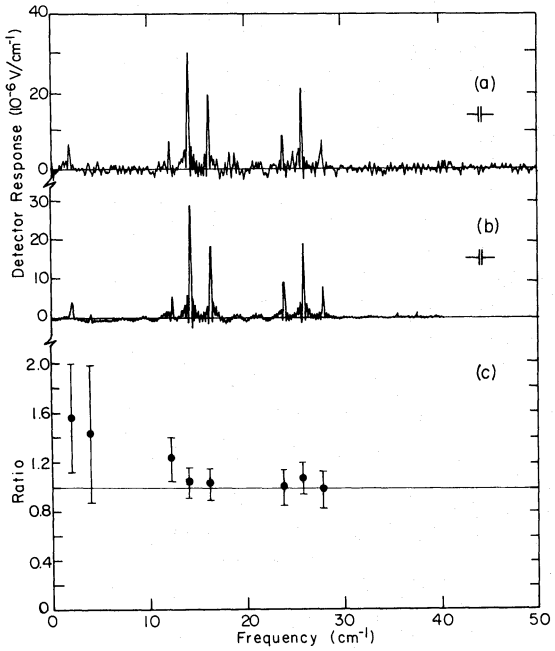

FIG. 12.—(*a*) Measured spectrum of the atmospheric O_2. (*b*) Calculated spectrum of the atmospheric O_2 using the expected column density. (*c*) Ratio of the experimental O_2 peak heights to the calculated peak heights with $\pm 1\ \sigma$ error limits.

trum. The noise in the observed spectrum of the night sky is a random, spectrally uncorrelated source of error. The errors in the calculated atmospheric emission were treated as being uncorrelated from one emission line to the next. The correlated and uncorrelated errors are shown separately in Figure 11 and must be treated separately when fitting models to the observed CMB spectrum. The $\pm 1\ \sigma$ error range for the uncorrelated errors is shown by the hatched region. The $\pm 1\ \sigma$ limits obtained when the correlated errors are included are shown by the solid lines. The correlated errors were calculated by rescaling the measured instrumental responsivity by the estimated frequency-independent calibration error (i.e., +4% and −7%) and repeating the analysis, including the fit to the atmospheric model. This scales the measured flux up 7% or down 4% in regions where the atmospheric contribution to the observed night sky emission is small. In essence the hatched region can be scaled uniformly up or down within the solid lines for a 1 σ degradation of the data, while points separated by more than 1 cm^{-1} can be shuffled up or down randomly within the hatched region. There are gaps in the plot at the positions of strong atmospheric lines where the errors arising from the atmospheric emission are large. Table 2 lists 12 independent data points separated by 1.01 cm^{-1} along with their associated error limits.

TABLE 2

OBSERVED SPECTRUM OF THE CMB

Frequency (cm^{-1})	Spectral Flux (10^{-12} W/cm^2 sr cm^{-1}) Measured	Uncorrelated Errors $\pm 1\sigma$	All Errors $\pm 1\sigma$	Temperature (K) Measured	All Errors $\pm 1\sigma$	Atmospheric Contribution at 1.01 cm^{-1} Resolution (%)
2.38.....	8.74	±0.77	+1.25 −0.98	3.28	+0.29 −0.23	38
3.40.....	12.13	±0.79	+1.54 −1.11	3.09	+0.20 −0.14	10
4.41.....	14.81	±0.71	+1.70 −1.16	3.07	+0.15 −0.10	12
5.42.....	16.05	±0.72	+1.84 −1.24	3.06	+0.12 −0.09	<1
6.44.....	16.09	±0.69	+1.85 −1.23	3.05	+0.11 −0.07	1
7.45.....	13.89	±0.65	+1.68 −1.13	2.98	+0.09 −0.07	11
8.46.....	12.42	±0.63	+1.56 −1.06	2.98	+0.09 −0.06	14
9.48.....	8.63	±0.62	+1.26 −0.92	2.85	+0.09 −0.06	24
10.49.....	6.64	±0.62	+1.11 −0.83	2.83	+0.08 −0.07	33
11.50.....	5.52	±0.91	+1.22 −1.04	2.85	+0.10 −0.10	65
12.52.....	4.07	±1.37	+1.40 −1.38	2.83	+0.14 −0.17	87
13.53.....	4.92	±2.06	+2.23 −2.10	3.04	+0.19 −0.24	89

The spectrum of a 2.96 K blackbody, which has the same integrated flux as the observed CMB in the frequency range from 2.4 to 13.5 cm^{-1}, is shown as a solid line in Figure 11. The most striking feature of our data is the qualitative agreement with this Planck curve. The agreement covers nearly a decade in frequency and extends from the Rayleigh-Jeans to the Wien part of the spectrum.

VII. COMPARISON WITH PREVIOUS MEASUREMENTS

A variety of techniques have been used to observe the CMB over the frequency range from 10^{-2} to 10 cm^{-1}. These techniques can be divided into four categories: narrow-band microwave radiometry, observation of the optical absorption in interstellar CN molecules, broad-band near-millimeter radiometry, and near-millimeter spectrophotometry. The measurement reported in this paper is in the last category. The results obtained with these techniques are summarized below.

There have been many measurements of the CMB using ground based microwave radiometers. These are listed in Table 3 along with the estimated 1 σ errors. These data fit blackbodies in the range from 2.62 K to 2.90 K with a normalized χ^2 of less than unity. The best fit temperature is 2.77 K with a normalized $\chi^2 = 0.2$.

Observations of the optical absorption lines for the interstellar molecule CN have been used to determine the excitation temperature of this molecule at 3.79 and 7.58 cm^{-1} (Thaddeus 1972). These observations constitute an indirect measurement of the CMB at distant points in our Galaxy. The excitation temperature at 3.79 cm^{-1} is 2.93 ± 0.06 K (Thaddeus 1972) and at 7.58 cm^{-1} it is $2.9^{+0.4}_{-0.5}$ K (Hegyi, Traub, and Carleton 1974). Thaddeus (1972) has calculated the contribution to the excitation temperature from electron impact to be 0.15 ± 0.08 K. This decreases the measured value of the temperature of the CMB at 3.79 cm^{-1} to 2.78 ± 0.10 K.

Several groups have reported direct measurements of the CMB in the frequency range covered by our observations. These results have been tabulated by Danese and De Zotti (1977), and a critical discussion is given elsewhere (Richards 1980; Richards and Woody 1980). The results reported here have smaller error limits and are in agreement with most of the previous direct measurements, including our earlier work (Woody *et al.* 1975). The only previous significant direct near-millimeter measurement which might be in disagreement with the data in Table 2 is the 1 to 11.5 cm^{-1} observation by Muehlner and Weiss (1973*b*). They report an integrated flux corresponding to a blackbody temperature of $2.55^{+0.25}_{-0.45}$ K.

The microwave data, the CN data, the observation of Muehlner and Weiss (1973*b*), and our results are presented in Figure 13 as a plot of the blackbody temperature versus frequency. The measurement techniques all overlap in the frequency range around 3 cm^{-1}. The set of measurements consisting of the 3.79 cm^{-1} CN measurement corrected for electron heating, the four highest frequency microwave data points, the results of Muehlner and Weiss (1973*b*), and our 3.40 cm^{-1} point are in moderately good agreement. These seven measurements yield a temperature of 2.81 ± 0.07 K with a normalized χ^2 of 0.5. Analyzing pairs of measurements shows that they are consistent at the 10% or higher probability level. The data in Figure 13 show that a

TABLE 3

MICROWAVE MEASUREMENTS OF THE CMB

Frequency (cm^{-1})	Temperature (K)	Reference
0.0136–0.0207	3.7 ± 1.2	Howell and Shakeshaft 1967
0.033–0.066	2.5 ± 0.3	Pelyushenko and Stankevich 1969
0.047	3.2 ± 0.33[a]	Penzias 1968
0.0483	2.8 ± 0.6	Howell and Shakeshaft 1966
0.136	3.3 ± 0.33[a]	Penzias 1968; Penzias and Wilson 1965
0.31	$2.69^{+0.16}_{-0.21}$	Stokes *et al.* 1967
0.313	3.0 ± 0.5	Roll and Wilkinson 1966
0.633	$2.78^{+0.12}_{-0.17}$	Stokes *et al.* 1967
0.667	2.0 ± 0.4[b]	Welch *et al.* 1967
1.08	3.16 ± 0.26	Ewing *et al.* 1967
1.17	$2.56^{+0.17}_{-0.22}$	Wilkinson 1967
1.22	2.9 ± 0.7	Puzanov *et al.* 1968
2.79	2.4 ± 0.7	Kislyakov *et al.* 1971
3.0	2.61 ± 0.25	Miller *et al.* 1971
3.0	$2.46^{+0.40}_{-0.44}$	Boynton *et al.* 1968
3.0	$2.46^{+0.50}_{-0.54}$	Boynton and Stokes 1974

[a] These errors are one-third of the error limits given by Penzias (private communications).

[b] These errors are one-half of the 95% confidence limits given by the authors.

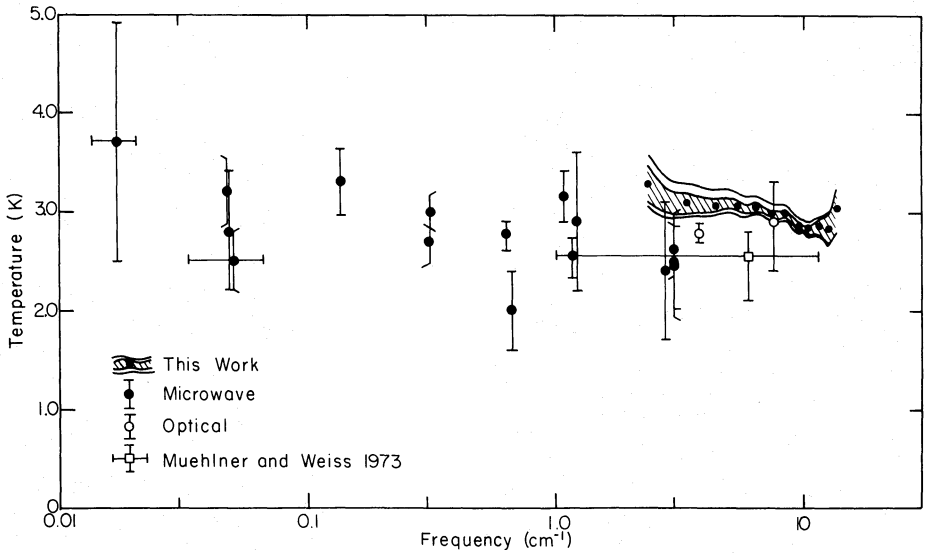

FIG. 13.—CMB measurements from Tables 2 and 3 plotted as temperature versus frequency

single blackbody temperature fits the observations made using a variety of techniques remarkably well over a frequency range of three decades.

VIII. MODEL FITTING

With the general blackbody nature of the CMB established well into the Wein limit where the exponential cutoff is dominant, it is appropriate to ask how accurately the observations fit a Planck spectrum. We have carried out a series of fits of the data to various models including a sample blackbody, a blackbody with temperature and emissivity as free parameters, and models of possible deviation based upon partial rethermalization of the CMB after its initial creation.

The uncertainties in our measurement of the CMB include both random and spectrally correlated errors which must be treated properly in order to correctly interpret the results from any model fitting. If the measurement is treated as a single measurement of the integrated flux from the CMB in the frequency range from 2.4 to 13.5 cm^{-1}, then the upper and lower flux limits (determined by integrating the area under the outer error limits are 1.1×10^{-10} and 1.4×10^{-10} W cm^{-2} sr^{-1}. Blackbodies at temperatures of 2.88 and 3.09 K would have the same integrated flux in this frequency range.[1]

A more complicated procedure is required to account for the spectral information contained in the data. The χ^2 statistic for the fit of a particular model to the data points in Table 2 is calculated according to the following formula:

$$\chi^2=\sum_{i=1}^{12}\left(\frac{\eta y_i-f_i}{\eta\sigma_i}\right)^2, \tag{4}$$

where y_i is the measured flux, f_i is the flux calculated from the model, σ_i is the estimated random error and η is a scale factor which is treated as a model parameter. The measured value of η is unity with standard deviation σ_η equal to the estimated spectrally correlated calibration error, i.e., 0.04 for $\eta<1$ and 0.07 for $\eta>1$. The probability of obtaining a particular value of χ^2 and η is then given by

$$P(\chi^2,\eta)\propto\exp\left\{-\tfrac{1}{2}\left[(2\chi^2)^{1/2}-(2n-1)^{1/2}\right]^2-\tfrac{1}{2}\left[1-\eta)/\sigma_\eta\right]^2\right\}, \tag{5}$$

where the normal approximation to the probability density for χ^2 with n degrees of freedom has been used (Martin 1971, p. 58). When the results from other measurements were included in the data set to be fit, their contribution to χ^2 was added to the χ^2 calculated above. The best fit is determined by minimizing the quantity

$$U^2=\left[(2\chi^2)^{1/2}-(2n-1)^{1/2}\right]^2+\left(\frac{1-\eta}{\sigma\eta}\right)^2. \tag{6}$$

Initially, we will discuss the fitting done using only our recent data. The temperature of the best fit

[1]These limits obtained from the integrated flux are more conservative than those quoted previously (Woody and Richards 1979) which were obtained by exploring the rate of increase of χ^2 as the blackbody temperature was changed from the best fit value.

blackbody is 2.90 K. This value is to be contrasted with the temperature of 2.96 K obtained from the integrated flux with the scale factor equal to 1.0. The two-parameter fit yielded a value of $U=2.7$ and $\eta=0.92$. There is only a 0.3% probability that a value of U larger than this would occur by chance.[2] The data thus show a statistically significant deviation from a simple Planck curve. The observations vary smoothly from ~10% above a 2.96 K Planck spectrum at 6 cm^{-1} to ~20% below it at 11 cm^{-1}. Although the deviations are not very much larger than the estimated error at any single point in the observations, their statistical significance accumulates because the deviation occurs at many independent spectral points. The magnitude of the deviation seen here is too small to have shown up in our earlier measurements of the near-millimeter CMB (Woody *et al.* 1975).

The possibility of atmospheric emission accounting for the observed deviation from a Planck spectrum has been investigated. The calculated atmospheric contribution is less than 40% of the observed night sky emission at 11 cm^{-1} where the CMB is 20% less than the 2.96 K Planck spectrum. Thus, a more than 30% error in the atmospheric model is required to remove the deficit at 11 cm^{-1}. The calculated atmospheric emission is less than 10% in the frequency range from 4 to 8 cm^{-1}, so an additional source of radiation is required to explain the excess in this region. Preliminary results from an independent measurement of the atmospheric emission at a similar altitude show no unexpected emission lines in this frequency range (Carli 1979), and no significant structure of the type expected for molecular emission is seen in the CMB spectrum at resolutions as fine as 0.13 cm^{-1}. Broad-band emission from water vapor dimers and wings from high-frequency lines, which may be present at mountain-top and airplane altitudes, are completely negligible at the 2 mbar float pressure of our measurement.

Limits on the atmospheric contribution to the observed flux can be determined by looking for correlations with the air mass along the line of sight. The float pressure and zenith angle were used to divide the interferograms into five groups according to air mass. The atmospheric fitting procedure was carried out separately for each group, and the integrated flux remaining after subtraction of the calculated atmospheric emission was determined. The fitted column densities and integrated flux are plotted in Figure 14 as a function of air mass. The error bars are the $\pm 1\ \sigma$ limits arising from the noise

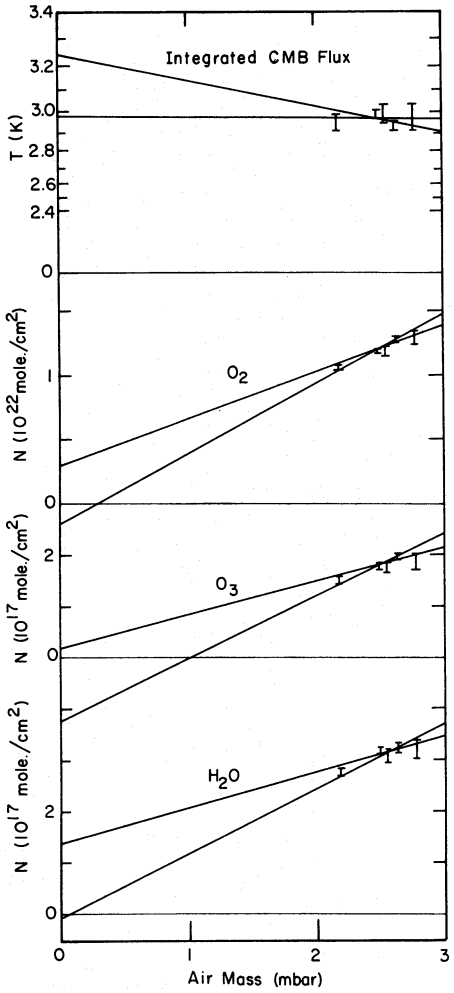

FIG. 14.—Fitted molecular column densities and integrated CMB flux as a function of air mass along the line of sight. The lines indicate the range of straight lines which fit the data.

in the measured interferogram. The integrated flux is plotted as an equivalent blackbody temperature with an ordinate scale which is linear in integrated flux. The pairs of straight lines correspond to the range of fitted striaght lines which have a normalized $\chi^2<1$. Although the uncertainties are large, the fact that the range of the straight lines in the column density plots includes the origin clearly shows that the data are consistent with column densities which are proportional to the air mass, while the integrated CMB flux is comparatively independent of air mass. There is only a 10% probability that the CMB data are consistent with a straight line whose intercept is 2.77 K, even when the calibration errors are included. This probability increases to 15% when a term proportional to the square root of the air mass is included which would be the case if a contribution from saturated atmospheric lines were present in

[2]The larger statistical significance of this deviation which was reported previously (Woody and Richards 1979) was the result of a faulty analysis procedure in which the standard deviations deduced from χ^2 and η were added linearly, instead of quadratically as is done here. Dr. J. Mather has pointed out that the points in Table 3 are too closely spaced to be statistically independent. Including the correlation of 0.16 between points reduces the value of χ^2 computed from equation (4) by a factor 0.77. Values of χ^2 and U throughout the paper have been adjusted accordingly.

the experimental measurement of the integrated CMB flux.

Several other local causes for the deviation from a Planck spectrum were also investigated. It is seen in all of the scans (which cover ~1.7 sr of the sky) and thus the possibility of a few bright sources is eliminated. Common types of interferometer ghosts were also shown to be negligible. The deviation does not fit a power-law spectrum with positive spectral index, and its magnitude is much larger than the continuum emission expected from the apparatus, from the Earth, or from galactic dust clouds. Most materials including plastics, metals, dust, and aerosols have emissivities which increase with frequency. Warm objects thus would produce an excess at the high frequencies—contrary to what we see. A limit of $0.2\times10^{-12}\times\nu$[W/cm^2 sr cm^{-1}] from a continuum was obtained by including a power law contribution in the model fitted to the observed night sky emission. The limit is smaller for spectral indices greater than unity. A cold absorber would have to have a physical temperature below 3 K to produce the observed deficit at 11 cm^{-1}. The apparatus is cold enough, but the possibility that there was a broad-band absorber such as ice in the spectrophotometer, which was present only during the flight, is not consistent with the in-flight calibration based upon the column density of O_2.

The poor fit of our data to a Planck spectrum is not altered significantly when the complete set of data consisting of the microwave measurements in Table 3, the optical CN measurements, the broad-band measurement of Muehlner and Weiss (1973*b*), and the spectrophotometer data in Table 2 are used. The best fit temperature is 2.88 K with $U=2.6$. Thus, there is less than 1% probability of all the data being consistent with a simple blackbody spectrum.

The simplest cosmological models of an expanding universe predict blackbody radiation based on very few assumptions. These models fail, however, to predict many gross features of the universe. Reality is clearly more complicated. Deviations from the Planck curve are expected at some level, and their observation is of highest importance for the refinement of cosmological models.

Compton scattering of the CMB by "hot" electrons, radiation damping of turbulence, and annihilation of matter and antimatter are some of the mechanisms which could lead to deviations from a blackbody spectrum (Zel'dovich, Illarionov, and Sunyaev 1972). The net result of these mechanisms is to scatter low-energy photons to higher energy and hence to shift the peak in the spectrum to higher frequencies. These models do not fit the data as well as a simple Planck curve. The best fit value of U is increased to four standard deviations for an energy exchange between the photons and an optically thin hot plasma equal to 4% of the energy in the CMB at the time of interaction.

This type of distortion is part of a general class which can be represented as a linear superposition of Planckian spectra of different temperatures of the form

$$F(\nu)=2hc^2\nu^3\int R(T)\frac{1}{\exp(hc\nu/kT)-1}dT, \quad (7)$$

with the weighting function $R(T)$ positive and normalized to unity (Zel'dovich, Illarionov, and Sunyaev 1972). The complete set of observations does not fit a function of this form even when the normalization restriction is removed. The difficulty is that the observed value of $\partial \ln F(\nu)/\partial\nu$ at high frequencies limits the highest temperature at which $R(T)$ can be significant to T_M ~2.7 K. Equation (7) then predicts a maximum value for the ratio of the spectral flux at two frequencies ν_1 and ν_2, with $\nu_1>\nu_2$, given by

$$\left[\frac{F(\nu_1)}{F(\nu_2)}\right]_{\max}=\frac{\nu_1^3}{\nu_2^3}\frac{\exp(hc\nu_2/kT_M)-1}{\exp(hc\nu_1/kT_M)-1}. \quad (8)$$

The observations exceed this ratio when the spectral flux in the region around 10 cm^{-1} is compared to the low frequency spectral flux, and thus they are inconsistent with a superposition of Planckian spectra.

The number density of photons in the CMB will be described by a Bose-Einstein distribution with a finite chemical potential if the photons reach thermal equilibrium with a hot gas through photon-conserving interactions, or if the photons have a finite rest mass. Including a parameter for a positive chemical potential does not improve the fit. A chemical potential of 3×10^{-18} ergs degrades the fit to $U=4$ standard deviations.

Some cosmological models which allow physical constants to vary as the universe evolves predict a Planck spectrum for the CMB with an effective emissivity which depends upon when thermal equilibrium was last established (Noerdlinger 1973; Narlikar and Rana 1980). A Planck spectrum with temperature and emissivity as free parameter satisfactorily fits the spectrophotometer data in Table 2. Blackbodies ranging from a temperature of 2.62 K with an emissivity of 1.62 to a temperature of 2.82 K with an emissivity of 1.20 yield a value of U of less than one standard deviation. A constant emissivity unequal to unity does not improve the fit to the complete set of CMB measurements. A 10% change in the emissivity increases U from 2.6 to 3.6 standard deviations.

The possibility of a constant percentage error in the calibration curve has been carefully considered. No possible source of such an error has been identified. If it had occurred, it would destroy the agreement of our data with the accepted column density of O_2.

The feature which makes it difficult to construct a sensible model that fits the data is the sharp decrease in flux at frequencies above ~8 cm^{-1}. This can be mod-

eled functionally by adding a ν^2 term to the emissivity. A reasonable fit to the entire data set is obtained for a temperature of 3.15 K and an emissivity equal to $0.81-(3.5\times10^3\nu^2)$. The value of U for this fit was one standard deviation. An optically thin absorber which is physically colder than the CMB at the time of interaction could produce such an emissivity but is difficult to produce in standard big bang cosmology.

Models of the CMB which do not involve establishing complete thermal equilibrium, or which utilize frequency-dependent emission processes, are relatively unconstrained and can be made to fit the observations. Rowan-Robinson, Negroponte, and Silk (1979) have carried out calculations using the redshifted dust features from a pregalactic generation of stars to increase the CMB in the 3 to 8 cm^{-1} frequency range relative to that on either side of this range. They obtained a satisfactory fit to the observations by this method.

The data in Figure 13 show that the observations of the CMB are remarkably consistent with a single-temperature blackbody over a three-decade frequency range. Although there is a statistically significant deviation from a Planck spectrum, there are serious limitations to the statistical analysis where systematic errors are likely. It is clear that another generation of measurements with better accuracy is required before any deviation from a Planck spectrum can be firmly established.

The authors have profited from discussions with R. Weiss and J. C. Mather. Part of the apparatus for this experiment was developed for earlier experiments done in collaboration with J. C. Mather and N. S. Nishioka. Technical help from H. Primbsch, S. McBride, N. S. Nishioka, and the staff of the National Scientific Balloon Facility is gratefully acknowledged. This work was partially supported by the U.S. Department of Energy under contract W-7405-ENG-48, and by the Office of Space Sciences of the National Aeronautics and Space Administration.

APPENDIX A

USE OF AN UNCALIBRATED SPECTROPHOTOMETER TO DETERMINE THE TEMPERATURE AND EMISSIVITY OF A SOURCE

The functional dependence of the Planck blackbody spectrum on temperature and frequency can be used to independently determine the emissivity and temperature of a calibration source with variable temperature. This becomes practical when the spectral range of the calibration includes both the Rayleigh-Jeans and Wien limits of the Planck spectrum. The spectrum obtained by a spectrophotometer viewing a calibration source is

$$S_1(\nu)=R(\nu)[\varepsilon(\nu)H(T_1,\nu)-H(T_0,\nu)], \tag{A1}$$

where ν=frequency, $R(\nu)$=instrumental responsivity, $\varepsilon(\nu)$=calibrator emissivity, $H(T,\nu)$=spectral flux from a blackbody at temperature T, T_0=internal spectrophotometer reference temperature, and T_1, T_2, T_3=calibrator temperature. The flux from the internal reference is negligible if $T_0 \ll T_1, T_2$. Then the ratio of the spectra measured for two different calibrator temperatures is just the ratio of the Planck spectra:

$$r(\nu)=\frac{S_1(\nu)}{S_2(\nu)}=\frac{H(T_1,\nu)}{H(T_2,\nu)}, \quad T_0 \ll T_1, T_2. \tag{A2}$$

The value of this ratio will depend upon whether H is in the Rayleigh-Jeans or Wien part of the Planck spectra. In particular, the Rayleigh-Jeans limit gives

$$r_{RJ}(\nu)=T_1/T_2, \tag{A3}$$

while the Wien limit gives

$$r_W(\nu)=\exp\left[\frac{hc\nu}{k}\left(\frac{1}{T_2}-\frac{1}{T_1}\right)\right]. \tag{A4}$$

If we define

$$b=\frac{1}{T_2}-\frac{1}{T_1}=\frac{k}{hc\nu}\ln[r_W(\nu)]. \tag{A5}$$

Equations (A3) and (A5) can be solved for T_1 and T_2,

$$T_1 = \frac{r_{RJ} - 1}{b} \qquad T_2 = \frac{r_{RJ} - 1}{r_{RJ} b}. \tag{A6}$$

If the flux from the internal reference is not negligible, the ratio of differences between three calibration spectra can be used.

$$r'(\nu) = \frac{S_1(\nu) - S_3(\nu)}{S_2(\nu) - S_3(\nu)} = \frac{H(T_1, \nu) - H(T_3, \nu)}{H(T_2, \nu) - H(T_3, \nu).} \tag{A7}$$

For $T_3 < T_1$, T_2, the contribution from $H(T_3, \nu)$ becomes negligible at sufficiently high frequencies. Equation (A7) then reduces to equation (A4). Equation (A7) reduces in the Rayleigh-Jeans limit to

$$r'_{RJ} = \frac{T_1 - T_3}{T_2 - T_3}, \tag{A8}$$

which clearly reduces to (A3) for $T_3 \ll T_1$, T_2. When used in the two limits, equation (A7) provides two equations for the three unknown temperatures. The shape of $r'(\nu)$ between these two limits provides a third (but insensitive) constraint on the temperatures. For T_3, T_2, and T_1 in the ratios of 1 to 2 to 4, we found a maximum change in $r'(\nu)$ of less than 3% for a 10% change in T_1 while holding r'_{RJ} and b constant. There is the added problem that, at a given frequency ν_0, it is possible to have two different values of T_1 with the same $r'(\nu_0)$, r'_{RJ}, and b. Thus using this ratio of differences technique requires accurate determination of $r'(\nu)$ at several intermediate frequencies in addition to the limiting values.

The emissivity of the calibrator can also be determined if it can be operated at temperatures close to T_0. Then we have

$$r(\nu) = \frac{\varepsilon(\nu) H(T_1, \nu) - H(T_0, \nu)}{\varepsilon(\nu) H(T_2, \nu) - H(T_0, \nu)}, \tag{A9}$$

which yields

$$\varepsilon(\nu) = \frac{[1 - r(\nu)] H(T_0, \nu)}{H(T_1, \nu) - r(\nu) H(T_2, \nu)}. \tag{A10}$$

APPENDIX B

LINE EMISSION

The absorption coefficient for collision-broadened lines has been derived by Van Vleck and Weisskopf (1945). The line shape reduces to the Lorentz line shape for line widths $\Delta\nu$ much less than the resonant frequency ν, and the absorption coefficient per molecule can be written as

$$k_{ij}(\mu) = \Delta N_{ij}(T) M_{ij} \frac{\Delta\nu/\pi}{(\nu - \nu_{ij})^2 + \Delta\nu^2}. \tag{B1}$$

The temperature dependence is described by the first factor, $\Delta N_{ij}(T)$, which is the fractional difference in population between the upper and lower levels. The strength of the dipole moment is contained in the second factor, M_{ij}. The line strength, S, is the product of these first two factors. The third factor is the Lorentz line shape normalized to have an integrated area of unity.

The difference in population between the upper and lower levels is given by the Boltzmann distribution

$$\Delta N_{ij} = [1 - \exp(-hc\nu_{ij}/kT)]\, g_i \exp(-E_i/kT)/Q(T), \tag{B2}$$

where E_i is the energy of the lower level, g_i the statistical weight of the lower level, and $Q(T)$ is the rotational partition function. The partition function is given by

$$Q(T) \propto T^{\beta}, \tag{B3}$$

where $\beta = 1.5$ for H_2O and O_3 and $\beta = 1.0$ for O_2 (McClatchey *et al.* 1973).

The treatment of line emission from the atmosphere given by Goody (1964, p. 223) will be used in the following discussion. The optical depth is given by the integral of the absorption coefficient along the line of sight,

$$\tau(\nu) = \int_l k(\nu) N(z)\, dz, \tag{B4}$$

where $N(z)$ is the number of molecules per unit volume. This integral can be calculated in closed form if the following assumptions are made: (1) the molecular species of interest is uniformly mixed throughout the atmosphere; (2) the pressure varies exponentially with altitude; (3) the atmosphere is isothermal; and (4) the line width is proportional to pressure. The first three conditions are reasonably well met in the altitude range of interest for balloon based observations (U.S. Standard Atmosphere Supplement 1966). The collision-broadened line width scales linearly with the pressure, P, and inversely with the square root of the temperature (Goody 1964, p. 106):

$$\Delta\nu \propto P T^{-1/2}. \tag{B5}$$

The Doppler broadening is proportional to the line frequency and to the square root of the temperature. The O_2 lines have an additional broadening from the Zeeman splitting of the lines in the earth's magnetic field (Liebe, Gimmestad, and Hopponen 1977). The pressure broadening of the lines within the spectral range of our instrument is several times larger than the Doppler width or Zeeman splitting. In our calculation, the rms sum of these contributions was used for the line width $\Delta\nu_0$ at the balloon altitude and the net width was assumed to be proportional to pressure for the purpose of integrating along the line of sight. The resulting optical depth is

$$\tau(\nu) = \frac{S}{2\pi}\frac{D}{\Delta\nu_0} \ln\left[1 + \frac{\Delta\nu_0^2}{(\nu - \nu_{ij})^2}\right], \tag{B6}$$

where D is the integrated column density along the line of sight. The equivalent width, W, is then given by

$$W = 2\pi^{1/2}\Delta\nu_0 \Gamma\left(\frac{S}{2\pi}\frac{D}{\Delta\nu_0} + \frac{1}{2}\right) \Big/ \Gamma\left(\frac{SD}{2\pi\Delta\nu_0}\right). \tag{B7}$$

Unsaturated lines have $SD/2\pi\Delta\nu_0 \ll 1$, and the equivalent width reduces to

$$W = SD. \tag{B8}$$

Saturated lines have $SD/2\pi\Delta\nu_0 \gg 1$ and equivalent width

$$W = (2SD\Delta\nu_0)^{1/2}. \tag{B9}$$

The calculation of the flux emitted by a molecular line starts with the tabulated line strength at standard temperature and pressure. The line strength is scaled to the atmospheric temperature using the temperature dependence in equation (B2). The line width is scaled to the temperature and pressure at the balloon altitude using equation (B5). The equivalent width for a particular column density is then calculated using equation (B7). Finally the flux is obtained by multiplying W by the spectral flux for a blackbody at the temperature of the atmosphere and at the frequency of the molecular line.

It is instructive to calculate the temperature dependence of this flux in the Rayleigh-Jeans limit ($hc\nu_{ij}/kT \ll 1$) for both saturated and unsaturated lines. Most of the lines have small lower level energies so that the line strength is given by

$$S = \Delta N_{ij} M_{ij} \propto T^{-(\beta+1)}. \tag{B10}$$

The flux from unsaturated lines is

$$F=2SDckT\propto DT^{-\beta}, \tag{B11}$$

where $\beta=1.5$ for H_2O and O_3 and 1.0 for O_2. The Rayleigh-Jeans temperature dependence for a blackbody has been canceled by the Boltzmann distribution factor and we are left with the temperature dependence of the partition function. The flux from saturated lines is

$$F=2ckT(2SD\Delta\nu_0)^{1/2}\propto D^{1/2}T^{(1-2\beta)/4}. \tag{B12}$$

This gives a temperature dependence of $T^{-1/2}$ for H_2O and O_3 and $T^{-1/4}$ for O_2.

The column density fitted to an observed flux is $D\propto FT^{\beta}$ for unsaturated lines, and $D\propto F^2T^{(2\beta-1)/2}$ for saturated lines. To the extent that the important lines for a given gas are all saturated or all unsaturated, an error in the assumed temperature is exactly compensated by a shift in the fitted value of D. Partial compensation occurs even where this condition is not met.

REFERENCES

Bell, R. J. 1972, *Introduction to Fourier Transform Spectroscopy* (New York: Academic Press).
Boynton, P. E., and Stokes, R. A. 1974, *Nature*, **247**, 528.
Boynton, P. E., Stokes, R. A., and Wilkinson, D. T. 1968, *Phys. Rev. Letters*, **21**, 462.
Carli, B. 1979, private communication.
Danese, L., and De Zotti, G. 1977, *Nuovo Cimento*, **7**, 277.
Ewing, M. S., Burke, B. F., and Staelin, D. H. 1967, *Phys. Rev. Letters*, **19**, 1251.
Gebbie, H. A., Burroughs, W. J., and Bird, G. R. 1969, *Proc. Roy. Soc. London*, *A*, **310**, 579.
Goody, R. M. 1964, *Atmospheric Radiation*, Vol. **1** (Oxford: Clarendon Press).
Goorvitch, D. 1975, *Appl. Optics*, **14**, 1387.
Hegyi, D. J., Traub, W. A., and Carleton, N. P. 1974, *Ap. J.*, **190**, 543.
Howell, T. F., and Shakeshaft, J. R. 1966, *Nature*, **210**, 1318.
_____. 1967, *Nature*, **216**, 753.
Kakar, R. 1977, private communication.
Keller, J. B. 1962, *J. Opt. Soc. Am.*, **52**, 116.
Kislyakov, A. G. *et al.* 1971, *Soviet Astr.—AJ*, **15**, 29.
Lambert, D. K., and Richards, P. L. 1978, *Appl. Optics*, **17**, 1595.
Liebe, H. J., Gimmestad, G. G., and Hopponen, J. D. 1977, *IEEE Trans.*, **AP25**, 327.
Martin, B. R. 1971, *Statistics for Physicists* (New York: Academic Press).
Martin, D. H., and Puplett, E. 1969, *Infrared Phys.*, **10**, 105.
Mather, J. C., Richards, P. L., and Woody, D. P. 1974, *IEEE Trans.*, **MTT-22**, 1046.
McClatchey, R. A. *et al.* 1973, AFCRL Atmospheric Absorption Line Parameter Compilation, AFCRL-TR-73-0096.
Millea, M. F., McColl, M., Pederson, R. J., and Vernon, F. L., Jr. 1971, *Phys. Rev. Letters*, **26**, 919.
Muehlner, D. J., and Weiss, R. 1973*a*, *Phys. Rev. D*, **7**, 326.
_____. 1973*b*, *Phys. Rev. Letters*, **30**, 757.
Narlikar, J. V., and Rana, N. C. 1980, *Phys. Letters*, **77A**, 219.
Nishioka, N. S., Richards, P. L., and Woody, D. P. 1978, *Appl. Optics.*, **17**, 1562.
Noerdlinger, P. D. 1973, *Phys. Rev. Letters*, **30**, 761.
Pelyushenko, S. A., and Stankevich, K. S. 1969, *Soviet Astr.—AJ*, **13**, 223.
Penzias, A. A. 1968, *IEEE Trans.*, **MTT-16**, 608.
Penzias, A. A., and Wilson, R. W. 1965, *Ap. J.*, **142**, 419.
Puzanov, V. I., Salomonovich, A. E., and Stankevich, K. S. 1968, *Soviet Phys. Astr.*, **11**, 905.
Richards, P. L. 1980, *Phys. Scripta*, **21**, 610.
Richards, P. L., and Woody, D. P. 1980, in *IAU Symposium 92, Objects of High Redshifts*, ed. G. Abell and J. Peebles (Dordrecht: Reidel), p. 283.
Roll, P. G., and Wilkinson, D. T. 1966, *Phys. Rev. Letters*, **16**, 405.
Rowan-Robinson, M., Negroponte, J., and Silk, J. 1979, *Nature*, **281**, 635.
Stokes, R. A., Partridge, R. B., and Wilkinson, D. T. 1967, *Phys. Rev. Letters*, **19**, 1199.
Thaddeus, P. 1972, *Ann. Rev. Astr. Ap.*, **10**, 305.
Tinkham, M., and Strandberg, M. W. P. 1955. *Phys. Rev.*, **97**, 937.
U.S. Standard Atmosphere Supplement 1966 (Environmental Science Services Administration, NASA).
Van Vleck, J. H., and Weisskopf, V. F. 1945, *Rev. Mod. Phys.*, **17**, 227.
Welch, W. J., Keachie, S., Thornton, D. D., and Wrixon, G. 1967, *Phys. Rev. Letters*, **18**, 1068.
Wilkinson, D. T. 1967, *Phys. Rev. Letters*, **19**, 1195.
Winston, R. 1970, *J. Opt. Soc. Am.*, **60**, 245.
Woody, D. P. 1975, Ph. D. thesis, University of California, Berkeley.
Woody, D. P., Mather, J. C., Nishioka, N. S., and Richards, P. L. 1975, *Phys. Rev. Letters*, **34**, 1036.
Woody, D. P., and Richards, P. L. 1979, *Phys. Rev. Letters*, **42**, 925.
Zel'dovich, Y. B., Illarionov, A. F., and Sunyaev, R. A. 1972, *Zh. Eksp. Teor. Fiz.*, **35**, 643 (English transl. in *Soviet Phys.—JETP*, **62**, 1217 [1972]).

PAUL L. RICHARDS: Department of Physics, University of California, Berkeley, CA 94720

DAVID P. WOODY: Department of Physics, California Institute of Technology, Pasadena, CA 91125